Proceedings of *RAGtime 20–22, 15–19 Oct., 16–20 Sept., 19–23 Oct., 2018/2019/2020, Opava, Czech Republic*
Z. Stuchlík, G. Török and V. Karas, editors, Silesian University in Opava, 2020, pp. 73–82

Proton acceleration in the active galactic nuclei

Yakov Istomin[1] and Alexey Gunya[1,a]

[1]P.N. Lebedev Physical Institute, Leninsky Prospect 53, Moscow 119991, Russia
[a]aagunya@lebedev.ru

ABSTRACT

In this paper, the process of acceleration of an ultrahigh-energy proton in the active galactic nucleus is briefly considered. The full cycle of collisionless acceleration of a proton up to the maximum energy E_{max} includes the primary acceleration in the region of the light cylinder up to the energy $E_{max}^{2/3}$ and additional acceleration in the region of the relativistic jet base where the proton reaches its maximum energy E_{max}. Different regimes of acceleration of protons in a jet have been discovered, depending on the values of the amplitudes of the electric and magnetic fields. The obtained theoretical estimates were confirmed by the data of the Pierre Auger collaboration, as well as by the IceCube collaboration when evaluating the neutrino energy on a jet subparsec scale.

Keywords: Cosmic rays – active galactic nuclei – black holes

1 INTRODUCTION

High-energy protons make up up to 90% of the composition of ultra-high-energy cosmic rays. The most probable sources and mechanisms of origin of protons with energies $> 10^{19}$ eV has been an extensive discussion for decades. The detection of protons of such energies is hampered by the remoteness of objects, as well as by the natural dissipation of relic radiation by photons, called the Greisen-Zatsepin-Kuzmin effect. The most likely candidates for high-energy proton sources are active galactic nuclei (AGN), the astrophysical scales of which make it possible to form an optimal accelerating medium. It is assumed that the most likely mechanism responsible for the proton reaching such energies is stationary acceleration by an electric field in the vicinity of massive objects such as supermassive black holes (SMBH). This mechanism allows the proton to reach energies $> 10^{20}$ eV, due to the presence of weak magnetization with magnetic fields in the vicinity of the SMBH, as well as a large potential difference between the SMBH and the relativistic jet. The explanation of this mechanism is based on the Blandford-Znaek process (Blandford and Znajek (1977)). This is based on the assumption of extracting rotational energy from the SMBH. For comparison, Fermi acceleration of a proton on a shock wave can reach no more than 10^{15} eV (F. A. Aharonian. (2004)). The detection of high-energy protons is less bright and more difficult due to the much lower synchrotron losses compared to electrons. This is also an advantage when reaching the ultimate energies.

The calculations used a kinetic approach to describe the motion of a charged particle. This is a key difference from MHD modeling, since in the kinetic approach, the action of inertial forces is important, especially in the area of the light cylinder.

2 ELECTROMAGNETIC FIELD

Acceleration process starts from the inner boundary of the ISCO disk (Istomin and Sol (2009)). Due to turbulent accretion the primary protons achieved 10-100 eV. With an increase in the accretion rate $\dot{M}$, a part of the accreting matter forms a jet propagating along the axis of rotation of the BH. In terms of the topology of the electromagnetic field, the SMBH has a uniform split-monopole structure. A toroidal field arises in the magnetosphere, which, due to the slower decay of $B_\phi \simeq r^{-1}$ in comparison with the poloidal field $B_r \simeq r^{-2}$, reaches a significant value in the region where matter reaches relativistic velocities namely light cylinder (Fig. 1). This specific area where the electric field becomes equal to the magnetic field $E = H$ and linear velocity v becomes equal to light velocity c. Due to centrifugal force the proton shifting to the light cylinder surface and its energy increase asymptotically. A similar structure is well known in neutron stars (Goldreich and Julian (1969)).

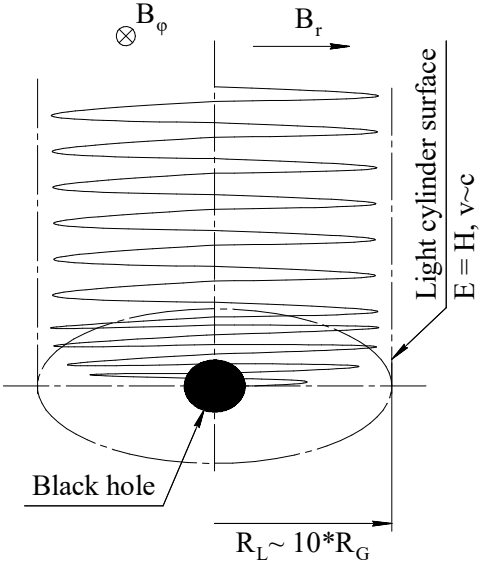

Figure 1. The magnetic field structure in the light cylinder

A relativistic jet is formed in the SMBH region of the corona above the surface of the light cylinder. In this region, the electromagnetic field is also inherited from the magnetosphere B_r, B_ϕ, E_θ into the jet B_z, B_ϕ, E_ρ. The structure of the magnetosphere electromag-

netic field is fully described in the work Istomin and Gunya (2020a), the structure of the jet electromagnetic field is fully described in the work Istomin and Gunya (2020b).

3 PARTICLE ACCELERATION

The trajectory of a full cycle of proton acceleration is the sum of the acceleration in the magnetosphere and the acceleration in the jet. The centrifugal force due to acceleration shifted the proton to the light cylinder with radius $R_L = \Omega_F/c$, where c is the speed of light, the magnetic field angular velocity Ω_F is determined by the angular velocity of the SMBH Ω_H as $\Omega_F \simeq \Omega_H/2$ (Blandford and Znajek (1977)). When the proton reaching the light cylinder, the energy increases to $\gamma_{max}^{(2/3)}$ asymptotically shifted to the boundary of the light cylinder and then leaves it, passing into the jet region. The pre-accelerated proton begins to increase its energy up to the maximum value $\gamma_{max}^{(1)}$ when it reaches the plane of intersection of the parabolic and conical jet profiles (Kovalev et al. (2020)). Upon reaching and crossing the jet boundary, the proton passes through the maximum potential difference, which gives the maximum energy.

The motion of particles with mass m and charge q in an electromagnetic field is described by the equations

$$\begin{aligned} \frac{\mathrm{d}\mathbf{p}}{\mathrm{d}t} &= q\left(\mathbf{E} + \frac{1}{c}[\mathbf{v},\mathbf{B}]\right), \\ \frac{\mathrm{d}\mathbf{r}}{\mathrm{d}t} &= \frac{\mathbf{p}}{m\gamma}, \\ \gamma^2 &= 1 + \frac{p^2}{m^2c^2}. \end{aligned} \tag{1}$$

Here $\mathbf{r}$ and $\mathbf{p}$ are coordinates and momentum of a charged particle, γ is its Lorentz factor.

The motion of a proton in the magnetosphere (Istomin and Gunya (2020a)) is described by equations (3). Here $\mathbf{r}$ and $\mathbf{p}$ are the coordinate and the momentum of a particle, γ is its Lorentz factor. It is convenient for us to introduce dimensionless time, coordinates, velocity and momentum,

$$t' = \frac{\omega_c t}{\gamma_i},\ \mathbf{r}' = \frac{\mathbf{r}}{r_L},\ \mathbf{v}' = \frac{\mathbf{v}}{c},\ \mathbf{p}' = \frac{\mathbf{p}}{mc\gamma_i}. \tag{2}$$

The initial value of the Lorentz factor is γ_i, the nonrelativistic cyclotron frequency of a particle rotation in the B_0 field is $\omega_c = qB_0/mc$. Let us also introduce the value of the Lorentz factor relative to the initial energy, $\gamma' = \gamma/\gamma_i$. In these variables, the equations of

motion (3) in spherical coordinates r, θ, ϕ (primes are omitted) have the form

$$\begin{aligned}
\frac{\mathrm{d}p_r}{\mathrm{d}t} &= \frac{\kappa}{r\gamma}\left(p_\theta^2 + p_\phi^2\right) + \frac{s\alpha}{r\gamma}p_\theta,\\
\frac{\mathrm{d}p_\theta}{\mathrm{d}t} &= -\frac{\kappa}{r\gamma}\left(p_r p_\theta - p_\phi^2\cot\theta\right) - \frac{s}{r}\sin\theta + \frac{s}{r^2\gamma}p_\phi - \frac{s\alpha}{r\gamma}p_r,\\
\frac{\mathrm{d}p_\phi}{\mathrm{d}t} &= -\frac{\kappa}{r\gamma}\left(p_r + p_\theta\cot\theta\right)p_\phi - \frac{s}{r^2\gamma}p_\theta,\\
\frac{\mathrm{d}r}{\mathrm{d}t} &= \frac{\kappa}{\gamma}p_r,\\
\frac{\mathrm{d}\theta}{\mathrm{d}t} &= \frac{\kappa}{r\gamma}p_\theta.
\end{aligned} \tag{3}$$

Here $s = sign|z|$.

The equations of a proton motion in a jet (Istomin and Gunya (2020b)) is described by equations (5).

The dimensionless time, coordinates and variables

$$\begin{aligned}
t' &= \frac{c}{R_J}t,\ \rho' = \frac{\rho}{R_J},\ z' = \frac{z}{R_J},\\
\mathbf{p}' &= \frac{c}{\omega_c R_J}\frac{\mathbf{p}}{mc},\ \gamma' = \frac{c}{\omega_c R_J}\gamma.
\end{aligned} \tag{4}$$

The value of ω_c is the nonrelativistic frequency of rotation of a particle in the magnetic field. The relation c/ω_c is the cyclotron radius of a nonrelativistic particle. It is significantly smaller than the jet radius R_J, $c/\omega_c R_J << 1$. Omitting the primes, we move to the equations of particle motion in the fields $B_z = B_0$, B_ϕ, E_ρ

$$\begin{aligned}
\frac{\mathrm{d}p_\rho}{\mathrm{d}t} &= \frac{p_\phi^2}{\rho\gamma} + \frac{p_\phi}{\gamma} - \alpha\frac{p_z\rho(1-\rho)^2}{\gamma} + \beta\rho(1-\rho)^2,\\
\frac{\mathrm{d}p_\phi}{\mathrm{d}t} &= -\frac{p_\rho p_\phi}{\rho\gamma} - \frac{p_\rho}{\gamma},\\
\frac{\mathrm{d}p_z}{\mathrm{d}t} &= \alpha\frac{p_\rho\rho(1-\rho)^2}{\gamma},\\
\frac{\mathrm{d}\rho}{\mathrm{d}t} &= \frac{p_\rho}{\gamma},\\
\frac{\mathrm{d}\phi}{\mathrm{d}t} &= \frac{p_\theta}{\rho\gamma},\\
\frac{\mathrm{d}z}{\mathrm{d}t} &= \frac{p_z}{\gamma}.
\end{aligned} \tag{5}$$

The dimensionless equations (3) and (5) uncluding dimensionless parameters. Magnetic field parameter $\alpha = B_\phi/B_0$, where B_0 is the radial field B_r for the magnetosphere or the

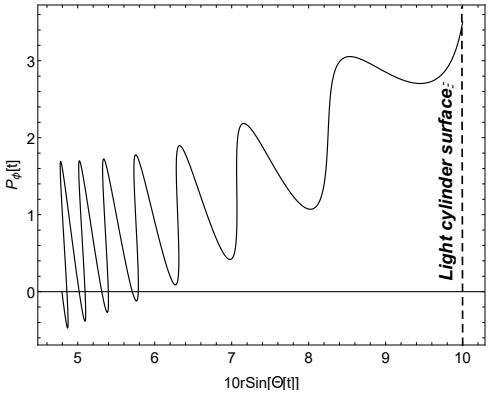

Figure 2. The magnetosphere toroidal momemtum versus the radial distance $r \sin\theta$. The numerical parameters considered as an example $\kappa = 10^{-2}$ and $\alpha = 10^{-2}$. The light cylinder surface is located at 10 on the abscissa axis.

longitudinal field B_z for the jet. The parameter of the electric field amplitude in the jet β and the magnetization parameter $\kappa = \Omega_F/\omega_c << 1$ in the magnetosphere, characterizing the cyclotron frequency of the particle ω_c much higher than the angular velocity of the magnetic field Ω_F.

Analysis of the toroidal moment P_ϕ on the figure (2) shows that centrifugal acceleration $P_\phi >> P_r + P_\theta$ is predominant in the area of the light cylinder R_L.

Analysis of the proton acceleration trajectory showed that the main energy increment occurs in the near-boundary region of the light cylinder (Fig. 3). The thickness of this area:

$$\Delta r = -\frac{s\kappa\gamma_{max}}{\sin^2\theta}\frac{p_r}{p_\theta}\,|_{r=1/\sin\theta}\,. \tag{6}$$

The calculation of the dependence of the proton energy on the distance to the light cylinder revealed that the proton leaves the acceleration region on the light cylinder when $\gamma_{max}^{(2/3)}$ is reached for the magnetosphere with a significant dominance of the toroidal field B_ϕ over poloidal B_r, which is typical for systems with AGN and a jet, and $\gamma_{max}^{(1/2)}$ for systems with an insignificant toroidal field, which is typical for inactive nuclei without a jet.

In a jet, the trajectory of displacement and the increment of energy occur mainly in the radial direction at different (Fig. 4).

Three acceleration regimes are determined depending on the values of the dimensionless amplitudes of the electric and magnetic fields.
(1) $\beta^2 - \alpha^2 > a_2^2 = 36$ – protons in the "untrapped" regime acquire the total energy $\gamma = \gamma_{max}$,
(2) $19 = a_1^2 < \beta^2 - \alpha^2 < a_2^2 = 36$ – protons in the "trapped" regime cyclically increase and lose energy, oscillating between the boundary and the axis of jet $\gamma = 0.74\gamma_{max}$,
(3) $\beta^2 - \alpha^2 < a_1^2 = 19$ – protons are not accelerated in the jet and move with the energy previously acquired in the magnetosphere, $\gamma = \gamma_{max}^{2/3}$ along the jet axis with insignificant oscillation.

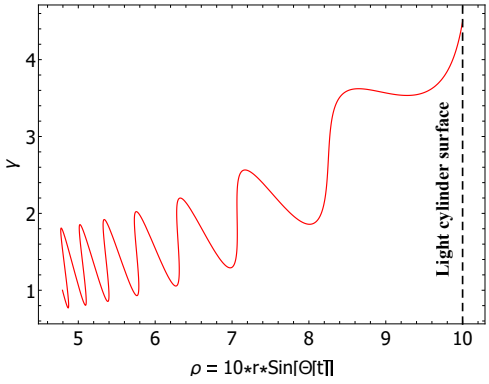

Figure 3. The magnetosphere Lorentz factor versus the radial distance $r \sin\theta$. The numerical parameters considered as an example $\kappa = 10^{-2}$ and $\alpha = 10^{-2}$. The light cylinder surface is located at 10 on the abscissa axis.

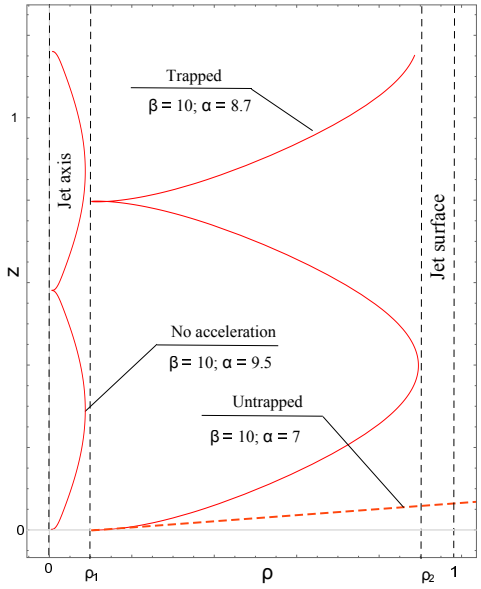

Figure 4. Particle trajectories on the plane (ρ, z). The figure shows particle trajectories in the regimes: untrapped, trapped and nonaccelerated.

4 AGN

The energy achieved in the magnetosphere and the jet, as well as the acceleration regime for a real AGN, is determined by the potential U generated by the SMBH and transferred along the magnetic field lines from the magnetosphere to the jet. Thus, the U is also the total potential difference between the region of the ergosphere of the SMBH in the

magnetosphere and the boundary of the jet. The SMBH potential (Thorne et al. (1986), Landau and Lifshitz (1984)) is

$$U = B_p r_g^2 \Omega_H / 2c. \tag{7}$$

The angular velocity of rotation of the black hole is proportional to the angular momentum of rotation of the black hole $J = j(M^2 G/c)$, where j is the specific angular momentum of the black hole, $j < 1$,

$$\Omega_H = \frac{2c}{r_g} \frac{j}{1 + (1 - j^2)^{1/2}}. \tag{8}$$

The quantity r_g is the gravitational radius of a SMBH with mass M,

$$r_g = \frac{2GM}{c^2} = 3 \cdot 10^5 \frac{M}{M_\odot} \text{ cm} = 3 \cdot 10^{14} M_9 \text{ cm}. \tag{9}$$

The value M_9 denotes the mass represented in units of $10^9 M_\odot$. Accordingly, $\Omega_H = 2 \cdot 10^{-4} M_9^{-1} j/[1 + (1 - j^2)^{1/2}]\ s^{-1}$.

The energies are defined as follows. For a proton accelerated in the "untrapped" regime, the energy is

$$E_{max}[\text{eV}] = 300 \cdot U[\text{cgs}]; \tag{10}$$

for a proton accelerated in the "trapped" regime, the energy is

$$E_{max}[\text{eV}] = 0.74 \cdot 300 \cdot U[\text{cgs}]; \tag{11}$$

and finally, for a proton moving in the "nonacceleration" regime

$$E_i[\text{eV}] = 0.94\,\text{GeV} \cdot \left(\frac{U[\text{eV}]}{0.94\,\text{GeV}} \right)^{2/3} \tag{12}$$

is the initial energy acquired in the magnetosphere. Parameters such as mass M_9, magnetic field B_4, specific angular momentum j, potential U, energies E_{max}, E_i.

5 SUMMARY

It has been proved that the main energy of the high-energy cosmic ray proton is accumulated in the region of the light cylinder R_L of the SMBH magnetosphere in the process of collisionless stationary electromagnetic acceleration. The astrophysical scales of the magnetosphere of the AGN core and its surroundings, including the jet and the inner boundary of the ISCO disk (Istomin and Sol (2009)), accelerate charged particles most effectively. The conversion of the rotational energy of the SMBH into the rotation of the magnetic field lines of the poloidal field B_p is possible thanks to the Blandford-Znajek process, direct numerical simulations of which (Komissarov (2001)), (Komissarov (2005)) confirmed the

Table 1. Enrgies and acceleration regimes in the AGNs

Object	E_{max} [eV]	E_i [eV]	regime
OQ 530	$3.6 \cdot 10^{19}$	$2.4 \cdot 10^{14}$	trap./untrapped
S5 2007+77	$5.1 \cdot 10^{19}$	$3.0 \cdot 10^{14}$	trap./untrapped
S4 0954+ 5	$8.4 \cdot 10^{19}$	$4.2 \cdot 10^{14}$	trap./untrapped
NGC 1275	$1.9 \cdot 10^{21}$	$3.3 \cdot 10^{15}$	untrap./trapped
NGC 4261	$1.4 \cdot 10^{20}$	$5.9 \cdot 10^{14}$	untrap./trapped
NGC 4486	$1.6 \cdot 10^{20}$	$6.4 \cdot 10^{14}$	untrap./trapped
3C 371	$1.3 \cdot 10^{21}$	$3.2 \cdot 10^{15}$	untrapped
3C 405	$9.6 \cdot 10^{20}$	$2.6 \cdot 10^{15}$	untrapped
NGC 6251	$2.9 \cdot 10^{21}$	$5.5 \cdot 10^{15}$	untrapped
3C 120	$4.0 \cdot 10^{21}$	$6.7 \cdot 10^{15}$	untrapped
BL Lac	$9.3 \cdot 10^{21}$	$1.2 \cdot 10^{16}$	untrapped
3C 273	$5.4 \cdot 10^{21}$	$6.7 \cdot 10^{15}$	untrapped
3C 390.3	$9.8 \cdot 10^{21}$	$1.2 \cdot 10^{16}$	untrapped
3C 454.3	$8.1 \cdot 10^{20}$	$1.9 \cdot 10^{15}$	trap./untrapped
1H 0323+342	$5.2 \cdot 10^{20}$	$1.7 \cdot 10^{15}$	untrapped
SS433	$6.7 \cdot 10^{20}$	$2.0 \cdot 10^{15}$	untrapped

efficiency and possibility of this process, as well as an immediate impact on the formation of a jet (Sob'yanin (2019)). The rotation of the poloidal magnetic field lines provides the generation of a polar electric field E_θ, which makes it possible to accelerate the proton to $\gamma_{max}^{(2/3)}$. The total potential difference U ends already at the jet boundary, where the radial electric field E_ρ is inherited from the initially generated SMBH polar field E_θ. In the "untrapped" regime, the proton escape out of the jet, accelerating to the limit value $\gamma_{max}^{(1)}$. In the table 1 shortly represented energies and regimes for diffrent real AGNs. The more complete set of parameters is presented in work Istomin and Gunya (2020b). The obtained data of the total energy E_{max} proton from table 1 also correspond to the data obtained from several sources by PA collaboration (Pierre Auger Collaboration and Abraham (2008)), (Abreu (2010)), (Nagar and Matulich (2008)), (Aab (2018)), (Zaw et al. (2009)). Note that due to natural constrains (Pierre Auger Collaboration and Abreu (2013)) named GZK-effect (Zatsepin and Kuz'min (1966)), not all sources can be associated with the predicted energies. Also according to IceCube results (Plavin (2020)), the neutrino energy in the subparsec region at the base of the jet corresponds to the maximum energy of colliding protons $E_p \simeq 10^{16} - 10^{17}$ eV, which corresponds to orders of magnitude energy acquired by protons in the region of the SMBH magnetosphere (third coloumn (Tab. 1)). Eventually the proton acceleration algorithm directly depends on the activity of the galactic nucleus (5).

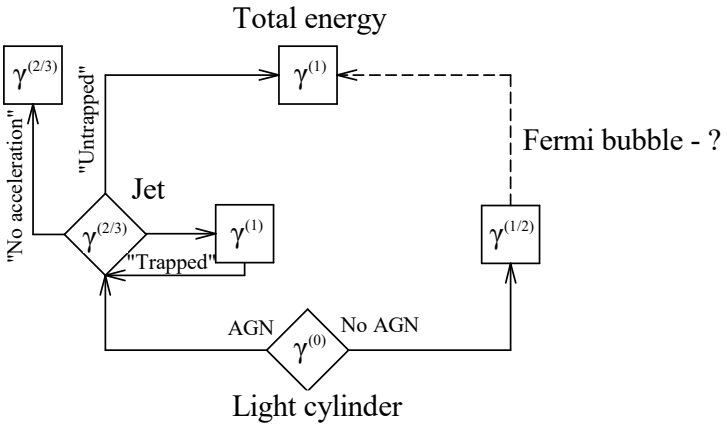

Figure 5. UHECR proton acceleration algorythm for diffrenet galaxyes activity

The acceleration of a proton in a non active nuclei to energy E^1_{max} is also assumed to possibly occur in a Fermi bubble, which will be considered by the authors in the next paper.

REFERENCES

Aab, A. e. a. (2018), An Indication of Anisotropy in Arrival Directions of Ultra-high-energy Cosmic Rays through Comparison to the Flux Pattern of Extragalactic Gamma-Ray Sources, *ApJ*, **853**(2), L29, arXiv: 1801.06160.

Abreu, P. e. a. P. (2010), Update on the correlation of the highest energy cosmic rays with nearby extragalactic matter, *Astroparticle Physics*, **34**(5), pp. 314–326, arXiv: 1009.1855.

Blandford, R. D. and Znajek, R. L. (1977), Electromagnetic extraction of energy from Kerr black holes., *MNRAS*, **179**, pp. 433–456.

F. A. Aharonian. (2004), High-energy particle acceleration in the shell of a supernova remnant, *Nature*, **432**(7013), pp. 75–77.

Goldreich, P. and Julian, W. H. (1969), Pulsar Electrodynamics, *ApJ*, **157**, p. 869.

Istomin, Y. N. and Gunya, A. A. (2020a), Centrifugal acceleration of protons by a supermassive black hole, *MNRAS*, **492**(4), pp. 4884–4891.

Istomin, Y. N. and Gunya, A. A. (2020b), Acceleration of high energy protons in agn relativistic jets, *Phys. Rev. D*, **102**, p. 043010, URL https://link.aps.org/doi/10.1103/PhysRevD.102.043010.

Istomin, Y. N. and Sol, H. (2009), Acceleration of particles in the vicinity of a massive black hole, *Astrophys. Space Sci.*, **321**, pp. 57–67.

Komissarov, S. S. (2001), Direct numerical simulations of the Blandford-Znajek effect, *MNRAS*, **326**(3), pp. L41–L44.

Komissarov, S. S. (2005), Observations of the Blandford-Znajek process and the magnetohydrodynamic Penrose process in computer simulations of black hole magnetospheres, *MNRAS*, **359**(3), pp. 801–808, arXiv: astro-ph/0501599.

Kovalev, Y. Y., Pushkarev, A. B., Nokhrina, E. E., Plavin, A. V., Beskin, V. S., Chernoglazov, A. V., Lister, M. L. and Savolainen, T. (2020), A transition from parabolic to conical shape as a common effect in nearby AGN jets, *Mon. Not. R. Astron. Soc.*, **495**(4), pp. 3576–3591.

Landau, L. D. and Lifshitz, E. M. (1984), *Course of Theoretical Physics. Vol. 8.*, Oxford.

Nagar, N. M. and Matulich, J. (2008), Ultra-high energy cosmic rays detected by the Pierre Auger observatory. First direct evidence, and its implications, that a subset originate in nearby radiogalaxies, *A&A*, **488**(3), pp. 879–885, arXiv: 0806.3220.

Pierre Auger Collaboration and Abraham, e. a. (2008), Correlation of the highest-energy cosmic rays with the positions of nearby active galactic nuclei, *Astroparticle Physics*, **29**(3), pp. 188–204, arXiv: 0712.2843.

Pierre Auger Collaboration and Abreu, P. e. (2013), Constraints on the Origin of Cosmic Rays above 10^{18} eV from Large-scale Anisotropy Searches in Data of the Pierre Auger Observatory, *ApJ*, **762**(1), L13, arXiv: 1212.3083.

Plavin (2020), Observational evidence for the origin of high-energy neutrinos in parsec-scale nuclei of radio-bright active galaxies, *Astrophys. J.*, **894**(2), 101.

Sob'yanin, D. N. (2019), Relativistic polytrope from the collimation and acceleration profiles of the M87 jet at subparsec scales and thermodynamic evidence for the Blandford-Znajek mechanism, *MNRAS*, **489**(1), pp. L7–L11, arXiv: 1908.05485.

Thorne, K. S., Price, R. H. and MacDonald, D. A. (1986), *Black Holes: the Membrane Paradigm.*, Yale University Press, New Haven.

Zatsepin, G. T. and Kuz'min, V. A. (1966), Upper Limit of the Spectrum of Cosmic Rays, *Soviet Journal of Experimental and Theoretical Physics Letters*, **4**, p. 78.

Zaw, I., Farrar, G. R. and Greene, J. E. (2009), Galaxies Correlating with Ultra-High Energy Cosmic Rays, *ApJ*, **696**(2), pp. 1218–1229, arXiv: 0806.3470.